



# Integrated dimensional and drive-train design optimization of a light-weight anthropomorphic arm

Lelai Zhou<sup>a,\*</sup>, Shaoping Bai<sup>a</sup>, Michael Rygaard Hansen<sup>b</sup>

<sup>a</sup> Department of Mechanical and Manufacturing Engineering, Aalborg University, Pontoppidanstræde 103, 9220 Aalborg, Denmark

<sup>b</sup> Department of Engineering, University of Agder, Grooseveien 36, 4876 Grimstad, Norway

## ARTICLE INFO

### Article history:

Received 30 December 2010

Received in revised form

15 September 2011

Accepted 19 September 2011

Available online 29 September 2011

### Keywords:

Integrated dimensional and drive-train optimization

Light-weight robot

Complex method

GCI

## ABSTRACT

An approach to minimize the mass of robotic manipulators is developed by integrated dimensional and drive-train optimization. The method addresses the influences of dimensions and characteristics of drive-trains in the design optimization. Constraints are formulated on the basis of kinematic performance and dynamic requirements, whereas the main objective is to minimize the total mass. Case studies are included to demonstrate the application of the optimization method in the design of assistive robots.

© 2011 Elsevier B.V. All rights reserved.

## 1. Introduction

Assistive robotic systems consisting of a robot arm mounting on a moving platform become increasingly important in assisting the handicapped and elderly people. Typical systems reported include FRIEND-I and FRIEND-II [1] from University of Bremen, KARES II [2], and RAPTOR [3]. For such systems, light-weight arms with high payload capacity are desirable from the point of view of both safety and energy efficiency. Specifically, it is desired that injuries caused by collision between robotic components and human beings are minimized in case of accidents.

The design of a light and strong robotic arm faces many challenges, varying from power supply, actuators, power transmission and structural parts. New technologies have been developed in connection with some novel robotic arms. DLR's robotics lab designed a 7-dof (degrees of freedom) torque-controlled light-weight robotic arm with a payload-to-weight ratio of 1 and a payload mass of 14 kg using customer designed drive-trains and carbon fiber structures [4]. Jardon et al. [5] built a 5-dof self-containing light-weight manipulator with a portable concept from wheelchair to docking stations in the room. Ananiev et al. [6] designed a 6-dof light-weight reconfigurable robotic arm mounted on a mobile platform. The 7-dof light-weight Whole Arm Manipulator (WAM)

developed by Barrett Technology takes advantage of differential mechanisms driven by cables and cylinder transmissions to reduce the effective arm inertia [7].

It is realized that the mass of an arm comes mainly from the structural parts and the drive-trains. A majority of research work in design optimization is related to the drive-train design. An early attempt on drive-train design optimization can be found in [8], in which Chedmail and Gautier proposed a method for the optimum selection of robot actuators to minimize the total mass of all the actuators. Pettersson and Ölvander [9] reported a method of design optimization, in which the drive-train of two joints was optimized for an industrial manipulator. A simulation environment called Modelica with robot optimization facilities was presented in [10], where the parameters of a controller were tuned by a multi-criteria parameter optimization method to improve the system dynamics. A drive-train optimization for robot designing was recently reported in [11]. The method is able to optimally select combinations of motors and gearboxes from a catalog of commercially available components for each dof of a robot arm. On the other hand, dimensional optimization was also studied for the improvement of robotic performance, either kinematic or dynamic one. An optimum robot design method based on a specified task was proposed [12], in which dimensions were optimized based on the dynamic analysis. A method to find optimal manipulator parameters using evolutionary optimization algorithms was presented in [13]. Methods based on optimal dynamic performance were reported in [14–17], among others, in which the influence of dimensions of robotic manipulators was rarely considered. It can be noticed that

\* Corresponding author.

E-mail addresses: [lzh@m-tech.aau.dk](mailto:lzh@m-tech.aau.dk), [lelaizhou@gmail.com](mailto:lelaizhou@gmail.com) (L. Zhou).

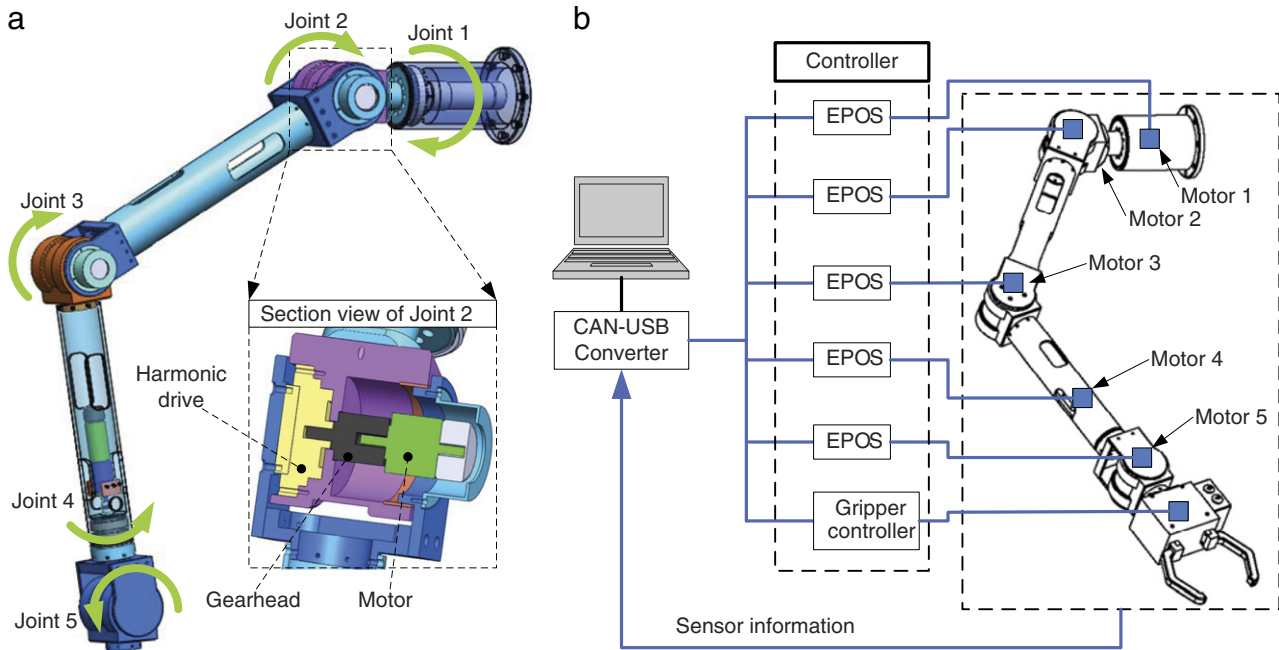


Fig. 1. (a) CAD rendering of a 5-dof light-weight anthropomorphic arm, (b) control system of the robotic arm.

in most of the research, dimensional and drive-train optimizations were conducted separately. An integrated approach is desired in order to fully utilize the potential of applying optimization techniques to the robot design.

This paper reports an integrated dimensional and drive-train optimization method for the design of robotic manipulators. Our interest is to include the dimensions of a robotic arm as variables in the design optimization, in addition to the parameters of the drive-trains. The inclusion of the dimensions in the optimization will allow us to account for their influence on the kinematic and dynamic performances, both being major concerns in the robot design. The work in this paper was carried out for a light-weight robotic arm of five degrees of freedom (dof), with two dof at the shoulder, one at the elbow, and two at the wrist, as shown in Fig. 1(a). This is a human-like arm design, which is to be mounted on an electric wheelchair to assist disabled people in simple manipulations like picking, placing, door opening, etc. For this purpose, a gripper is employed at the end of the arm, as demonstrated in Fig. 1(b). A design with minimal mass can make the robot intrinsically safe in assistive manipulations.

## 2. The anthropomorphic arm and modeling

The 5-dof robotic arm adopts a modular approach. As shown in Fig. 1(a), CPU series gearboxes of Harmonic Drive™ are used as transmission elements and, simultaneously, as the mechanical joints, for different dofs. To increase the torque capabilities of Joints 1–3, a second stage of gearhead is used between Harmonic Drive and the motor. The geared motors and Harmonic Drive gearboxes are mounted inside the joint housings, while the axes of rotation coincide with the joint axes, as illustrated in Fig. 1(a). The arm joints are driven by electrical motors, chosen among Maxon™ DC motors. The motors are equipped with encoders having 1000 counts per turn.

CANopen (Controller Area Network) bus is adopted for the communications between motors and controllers. As shown in Fig. 1(b), the motors are controlled by EPOS controllers, which are selected from Maxon. The gripper, selected from SOMMER™ Automatic, is controlled by its customized controller. CAN runs a two-wire differential serial communication protocol, the CANopen

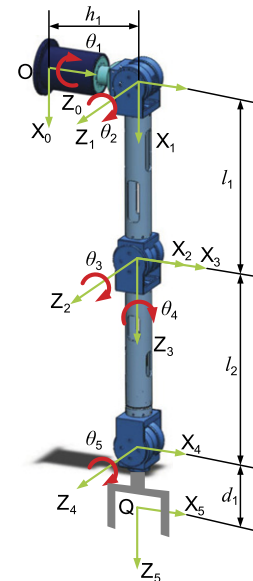


Fig. 2. Robotic arm coordinate systems.

protocol, for real-time control. CANopen protocol uses the CAN Physical Layer as defined by the CAN in Automation (CiA) standard ‘DS-301 Version 4.02’. The communications between CANopen bus and the PC are accomplished by a CAN–USB interface.

### 2.1. Kinematics

Following the Denavit–Hartenberg (D–H) convention [18], Cartesian coordinate systems are established for each link of the robotic arm, as shown in Fig. 2. D–H parameters are defined as listed in Table 1.

The transformation matrix in forward kinematics of the end-effector in fixed reference frame is given as

$${}^0A_5 = \begin{bmatrix} \mathbf{R} & \mathbf{q} \\ 0 & 1 \end{bmatrix} \quad (1)$$

with the rotation matrix  $\mathbf{R}$  and position vector  $\mathbf{q}$  given by

**Table 1**  
D–H parameters of the robotic arm.

Joint $i$	$\alpha_i$	$a_i$	$d_i$	$\theta_i$
1	$\pi/2$	0	$h_1$	$\theta_1$
2	0	$l_1$	0	$\theta_2$
3	$\pi/2$	0	0	$\theta_3$
4	$-\pi/2$	0	$l_2$	$\theta_4$
5	$\pi/2$	0	$d_1$	$\theta_5$

$$\mathbf{R} = \begin{bmatrix} u_x & v_x & w_x \\ u_y & v_y & w_y \\ u_z & v_z & w_z \end{bmatrix}, \quad \mathbf{q} = \begin{bmatrix} q_x \\ q_y \\ q_z \end{bmatrix}. \quad (2)$$

The joint angles for a given pose in terms of  $\mathbf{R}$  and  $\mathbf{q}$  can be found through the inverse kinematics. For simplicity, only solutions of the five joint angles are presented, which are

$$\theta_1 = \arctan\left(\frac{p_y}{p_x}\right), \quad 0 \leq \theta_1 \leq \pi \quad (3a)$$

$$\theta_3 = \arctan(s\theta_3, c\theta_3) \quad (3b)$$

where

$$\begin{aligned} p_x &= q_x - d_1 w_x, & p_y &= q_y - d_1 w_y, \\ p_z &= q_z - d_1 w_z \\ \kappa_1 &= l_1^2 + l_2^2, & \kappa_2 &= 2l_1 l_2, & \kappa_3 &= p_x^2 + p_y^2 + (p_z - h_1)^2, \\ \kappa_2^2 - (\kappa_3 - \kappa_1)^2 &> 0 \end{aligned}$$

$$s\theta_3 = (\kappa_3 - \kappa_1)/\kappa_2, \quad c\theta_3 = \sqrt{1 - ((\kappa_3 - \kappa_1)/\kappa_2)^2}.$$

Upon solved  $\theta_1$  and  $\theta_3$ , other joint angles are obtained as

$$\theta_2 = \arctan\left(\frac{(\mu_2 \eta_1 - \mu_1 \eta_2)(\zeta_2 \mu_1 - \zeta_1 \mu_2)}{(\mu_2 \zeta_1 - \mu_1 \zeta_2)(\zeta_2 \eta_1 - \zeta_1 \eta_2)}\right), \quad 0 \leq \theta_2 \leq \pi \quad (3c)$$

$$\begin{aligned} \theta_5 &= \arccos(w_x c\theta_1 s\theta_{23} + w_y s\theta_1 s\theta_{23} - w_z c\theta_{23}), \\ 0 &< \theta_5 < \pi \end{aligned} \quad (3d)$$

$$\theta_4 = \arctan(s\theta_4, c\theta_4) \quad (3e)$$

with

$$\begin{aligned} \mu_1 &= l_1 + l_2 s\theta_3, & \zeta_1 &= l_2 c\theta_3, & \eta_1 &= p_x c\theta_1 + p_y s\theta_1 \\ \mu_2 &= -l_2 c\theta_3, & \zeta_2 &= l_1 + l_2 s\theta_3, & \eta_2 &= p_z - h_1 \\ c\theta_4 &= \frac{w_x c\theta_1 c\theta_{23} + w_y s\theta_1 c\theta_{23} + w_z s\theta_{23}}{s\theta_5}, \end{aligned}$$

$$s\theta_4 = \frac{w_x s\theta_1 - w_y c\theta_1}{s\theta_5}, \quad s\theta_5 \neq 0$$

where  $c$  and  $s$  stand for harmonic functions cosine and sine, respectively. Moreover  $\theta_{23} \equiv \theta_2 + \theta_3$ .

## 2.2. Jacobian matrix

The joint angular velocity can be calculated with the Jacobian matrix

$$\dot{\boldsymbol{\theta}} = \mathbf{J}^{-1} \mathbf{v}_{ef} \quad (4)$$

where  $\dot{\boldsymbol{\theta}} = [\dot{\theta}_1, \dot{\theta}_2, \dots, \dot{\theta}_n]^T$  denotes an  $n$ -dimensional ( $n$  denotes the number of dof) vector of the joint angular velocities,  $\mathbf{J}$  is the Jacobian of the robotic arm, and  $\mathbf{v}_{ef}$  the velocity of the end-effector.

For a revolute joint, the Jacobian matrix can be calculated by [19]

$$\mathbf{J} = [\mathbf{j}_1, \mathbf{j}_2, \dots, \mathbf{j}_n], \quad \mathbf{j}_i = \begin{bmatrix} \mathbf{z}_{i-1} \times \mathbf{p}_{i-1} \\ \mathbf{z}_{i-1} \end{bmatrix} \quad (5)$$

where  $\mathbf{z}_{i-1}$  and  $\mathbf{p}_{i-1}$  are given by

$$\mathbf{z}_{i-1} = \mathbf{R}_{i-1} [0 \ 0 \ 1]^T, \quad \mathbf{p}_{i-1} = \mathbf{R}_{i-1} \mathbf{q}_{i-1} + \mathbf{p}_i \quad (6)$$

where  $\mathbf{q}_{i-1} = [a_i \cos \theta_i, a_i \sin \theta_i, d_i]^T$ ,  $\mathbf{R}_{i-1}$  denotes the rotation

matrix from the reference coordinate system to the  $(i - 1)$ th coordinate system. The local coordinates of the end-effector are defined as  $\mathbf{p}_n = [0, 0, 0]^T$ . When the desired end-effector velocity  $\mathbf{v}_{ef}$  is given, the joint angular velocity can be solved by Eq. (4).

## 2.3. Inverse dynamics

The integrated dimensional and drive-train optimization will make use of a dynamic model of the robotic arm for dynamic evaluations. The governing equation of the arm motion can be written as

$$\mathbf{M}(\boldsymbol{\theta}) \ddot{\boldsymbol{\theta}} + \mathbf{V}(\boldsymbol{\theta}, \dot{\boldsymbol{\theta}}) + \mathbf{G}(\boldsymbol{\theta}) = \boldsymbol{\tau} \quad (7)$$

where  $\mathbf{M}$  is the mass matrix,  $\mathbf{V}$  is the vector of Coriolis and centrifugal terms of the links,  $\mathbf{G}$  is the vector of gravitational forces,  $\boldsymbol{\tau}$  is the vector of joint torques, and  $\boldsymbol{\theta}$  is the vector of joint angles.

The mass matrix  $\mathbf{M}$  can be calculated as

$$\mathbf{M} = \sum_{i=1}^n (\mathbf{J}_{v,i}^T m_i \mathbf{J}_{v,i} + \mathbf{J}_{\omega,i}^T \mathbf{I}_i \mathbf{J}_{\omega,i}) \quad (8)$$

where  $\mathbf{J}_{v,i}$  and  $\mathbf{J}_{\omega,i}$  are  $3 \times n$  matrices. For revolute joint, the  $j$ th column vectors of  $\mathbf{J}_{v,i}$  and  $\mathbf{J}_{\omega,i}$  can be obtained by [19]

$$\mathbf{j}_{v,i}^j = \mathbf{z}_{j-1} \times \mathbf{p}_{c,i}^{j-1}, \quad \mathbf{j}_{\omega,i}^j = \mathbf{z}_{j-1}, \quad \text{for } j \leq i \quad (9a)$$

$$\mathbf{j}_{v,i}^j = \mathbf{j}_{\omega,i}^j = [0 \ 0 \ 0]^T, \quad \text{for } i < j \leq n \quad (9b)$$

where  $\mathbf{p}_{c,i}^{j-1}$  is a position vector defined from the origin of the  $j - 1$  link frame to the center of mass of link  $i$  and expressed in the base frame. Moreover,  $m_i$  and  $\mathbf{I}_i$  are the mass and the inertia matrix of the link  $i$ . For each link, its mass is found as

$$m_i = m_{s,i} + m_{m,i} + m_{g,i} \quad (10)$$

where  $m_{s,i}$  is the mass of the arm structure, which is proportional to the link length.  $m_{m,i}$  and  $m_{g,i}$  are the masses of motor and gearbox for the  $i$ th joint. Both  $m_i$  and  $\mathbf{I}_i$  vary with the selections of motors and gearboxes, and the link lengths as well.

## 3. Integrated dimensional and drive-train optimization

The integrated dimensional and drive-train optimization is proposed to minimize the mass of the robotic arm with constraints on kinematic performance and the robotic dynamics. The selection of motor and gearbox for a drive-train is constrained through the dynamic requirements and the selecting criteria for motors and gearboxes. Since the geometric dimensions<sup>1</sup> influence the robotic dynamics, and also determine the kinematic performance of the robotic manipulator; a constraint on the kinematic performance can be defined to account for the dimensions' influence.

With the objective to minimize the mass of the robotic arm, the optimization task is to find the lightest combination of motor and gearbox for all the joints and the optimal link lengths that fulfill all constraints associated with the kinematic performance, the motors and gearboxes. The optimization problem is defined as

$$\text{Minimize } f(\mathbf{x}) = \sum_{i=1}^n \{m_m(\mathbf{u}_m) + m_g(\mathbf{u}_g)\}_i \quad (11a)$$

$$\mathbf{x} = [\mathbf{u}_m, \mathbf{u}_g, \mathbf{u}_d]$$

$$\text{subject to } g_j(\mathbf{x}) \leq 0 \quad (11b)$$

where  $f(\mathbf{x})$  is the total mass of the robotic arm,  $g_j(\mathbf{x})$  is the set of inequality constraints. The array of design variable  $\mathbf{x}$  includes the index numbers of motors  $\mathbf{u}_m = [u_{m1}, \dots, u_{mn}]$  and gearboxes  $\mathbf{u}_g = [u_{g1}, \dots, u_{gn}]$ , relative to the database containing commercially available components, and an array of dimensional variables  $\mathbf{u}_d$ .

<sup>1</sup> Geometric dimensions in this work refer to the link lengths of the robotic arm's D–H parameters, namely,  $l_1$  and  $l_2$ .

The set of constraints  $g_j(\mathbf{x})$  includes the kinematic performance constraint, the constraints for motor selection, and that for gearbox selection, as described presently.

### 3.1. Global conditioning index

The kinematic performance is one of the major concerns in the robot design. It is desirable for a robot to have a high kinematic performance, while the drive-drain being optimized. Several performance indices have been used in designs of robotic manipulators. Yoshikawa [20] proposed manipulability measure as a metric of kinematic performance. Gosselin and Angeles [21] developed a global conditioning index (*GCI*) for the kinematic optimization of manipulators. The condition number and dexterity indices of the manipulator have been adopted in optimum designs [22–24].

Among the performance indices mentioned, the manipulability measure is a local performance measure and valid at a certain position only [25]. In this work, we use a global performance index, the global conditioning index (*GCI*). The *GCI* is defined over a workspace  $\Omega$  as [21]

$$GCI = \frac{\int_{\Omega} \frac{1}{\kappa} dW}{\int_{\Omega} dW} \quad (12)$$

with the condition number  $\kappa$  given by

$$\kappa = \|\mathbf{J}(\boldsymbol{\theta}, \mathbf{u}_d)\| \|\mathbf{J}^{-1}(\boldsymbol{\theta}, \mathbf{u}_d)\| \quad (13)$$

where  $\mathbf{J}(\boldsymbol{\theta}, \mathbf{u}_d)$  is the Jacobian matrix defined in Eq. (4). The Euclidean norm  $\|\cdot\|$  of the matrix is defined as

$$\|\mathbf{J}\| = \sqrt{\text{tr}(\mathbf{J}\mathbf{J}^T)} \quad (14)$$

with  $\mathbf{N} = \frac{1}{n}\mathbf{I}$ , where  $n$  is the dimension of the square matrix  $\mathbf{J}$ , and  $\mathbf{I}$  is the  $n \times n$  identity matrix.

In practice, the *GCI* of a robotic manipulator is calculated through a discrete approach as [26]

$$GCI = \frac{1}{W} \sum_{i=1}^m \frac{1}{\kappa_i} \Delta W_i \quad (15)$$

where  $W$  is the workspace volume, and  $m$  is the number of discrete points. In the case of equal-volumetric discretization,  $\Delta W_i \equiv \Delta W$ , Eq. (15) is simplified to

$$GCI = \frac{1}{m} \sum_{i=1}^m \frac{1}{\kappa_i}. \quad (16)$$

The *GCI* is dimension dependent, which means

$$GCI = GCI(\mathbf{u}_d). \quad (17)$$

To keep a high kinematic performance with selected link lengths in the integrated optimization, a constraint is given on the *GCI*

$$GCI(\mathbf{u}_d) \geq C_{\min} \quad (18)$$

where  $C_{\min}$  is a user-defined minimum acceptable *GCI*.

### 3.2. Drive-train modeling

A drive-train normally consists of a motor, a linkage and a gearbox for speed reduction. The drive-train model of a single robotic joint is shown in Fig. 3. For the Harmonic Drive gearbox, the gear efficiency varies relative to the output torque. The required motor torque for the  $i$ th joint is calculated by

$$\tau_{m,i} = \left\{ (J_m + J_g) \ddot{\theta}(t) \rho + \frac{\tau(t)}{\rho \eta_g} \right\}_i; \quad i = 1, \dots, n, \quad (19)$$

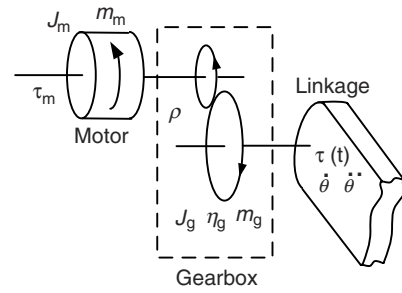


Fig. 3. Schematic view of drive-train model for a single joint.

where  $\rho_i$  is the gear ratio,  $J_{m,i}$  is mass moment of inertia of the  $i$ th motor,  $J_{g,i}$  is the equivalent mass moment of inertia of the  $i$ th gearbox,  $\eta_{g,i}$  is the corresponding gear efficiency, and  $\tau_i(t)$  is the load at the output link which can be solved by Eq. (7).

### 3.3. Motor selection criteria

In selecting motors, the following three constraints have to be satisfied, according to the motor selection criteria recommended by the manufacturer [27].

**Nominal torque limit.** The nominal torque is the so-called maximum continuous torque. The root mean square (RMS) value  $\tau_{rms}$  of the required motor torque  $\tau_m$  has to be smaller than or equal to the nominal torque of the motor  $T_m$

$$\tau_{rms} \leq T_m \quad (20)$$

where  $\tau_{rms} = \sqrt{\frac{1}{\Delta t} \int_0^{\Delta t} \tau_m^2 dt}$ , with  $\Delta t$  being the duration of a characteristic working cycle.

**Stall torque limit.** The stall torque is the peak torque of the motor. The required peak torque  $\tau_p$  has to be smaller than or equal to the stall torque  $T_m^{\max}$  of the motor

$$\tau_p \leq T_m^{\max} \quad (21)$$

where  $\tau_p = \max\{|\tau_m|\}$ .

**Maximum permissible speed limit.** The maximum permissible speed for DC motors is primarily limited by the commutation system. A further reason for limiting the speed is the rotor's residual mechanical imbalance which shortens the service life of the bearings. The required peak speed  $n_p$  corresponding to the motor has to be smaller than or equal to the maximum permissible speed  $N_m^{\max}$  of the motor

$$n_p \leq N_m^{\max} \quad (22)$$

where  $n_p = \max\{|2\pi \dot{\theta}(t) \cdot \rho|\}$ .

### 3.4. Gearbox selection criteria

In the selection of gearboxes, the following three constraints are considered:

**Rated output torque limit.** It is recommended by the Harmonic Drive gearbox manufacturer to use the RMC value for calculating rated torque [28]. The RMC value is a measure of the accumulated fatigue on a structural component and reflects typical endurance curves of steel and aluminum [29]. It is therefore relevant to gearbox lifetime, and this criterion has also been used in robotic applications [30]. With this criterion, a constraint is derived as

$$\tau_{rmc} \leq T_g \quad (23)$$

where  $\tau_{rmc} = \sqrt[3]{\frac{1}{\Delta t} \int_0^{\Delta t} \tau^3(t) dt}$ , with  $\tau(t)$  being the required torque from the gearbox output.  $T_g$  is the limit for rated torque of the gearbox.

**Maximum output torque limit.** The required peak torque  $\tau_g$  with respect to the output side has to be smaller than or equal to the allowable peak torque  $T_g^{\max}$  of the Harmonic Drive

$$\tau_g \leq T_g^{\max} \quad (24)$$

where  $\tau_g = \max\{|\tau(t)|\}$ .

**Maximum permissible input speed limit.** The required maximum input peak speed  $n_{in}$  has to be smaller than or equal to the maximum permissible input speed  $N_g^{\max}$  of a gearbox

$$n_{in} \leq N_g^{\max} \quad (25)$$

where  $n_{in} = \max\{|\dot{\theta}(t) \cdot \rho|\}$ .

### 3.5. Objective function formulation

Substituting Eq. (19) into Eqs. (20)–(21) and expanding Eqs. (22)–(25) yield the constraints on the motors and gearboxes. The objective function,  $f(\mathbf{x})$ , is formulated as

$$\min_{\mathbf{x}} f(\mathbf{x}) = \sum_{i=1}^5 \{m_m(\mathbf{u}_m) + m_g(\mathbf{u}_g)\}_i \quad (26a)$$

$$\mathbf{x} = [\mathbf{u}_m, \mathbf{u}_g, \mathbf{u}_d]$$

subject to

$$C_{\min} \leq GCI(\mathbf{u}_d) \quad (26b)$$

$$T_{m,i} \geq \sqrt{\frac{1}{\Delta t} \int_0^{\Delta t} \left\{ (J_m(\mathbf{x}) + J_g(\mathbf{x})) \ddot{\theta}(t) \rho + \frac{\tau(t, \mathbf{x})}{\rho \eta_g} \right\}_i^2 \cdot dt} \quad (26c)$$

$$T_{m,i}^{\max} \geq \max \left\{ \left| (J_m(\mathbf{x}) + J_g(\mathbf{x})) \ddot{\theta}(t) \rho + \frac{\tau(t, \mathbf{x})}{\rho \eta_g} \right|_i \right\} \quad (26d)$$

$$N_{m,i}^{\max} \geq \max \{ |2\pi \dot{\theta}(t) \cdot \rho|_i \} \quad (26e)$$

$$T_{g,i} \geq \sqrt[3]{\frac{1}{\Delta t} \int_0^{\Delta t} \tau_i^3(t, \mathbf{x}) \cdot dt} \quad (26f)$$

$$T_{g,i}^{\max} \geq \max\{|\tau(t, \mathbf{x})|_i\} \quad (26g)$$

$$N_{g,i}^{\max} \geq \max\{|\dot{\theta}(t) \cdot \rho|_i\} \quad (26h)$$

where  $T_{m,i}$ ,  $T_{m,i}^{\max}$ , and  $N_{m,i}^{\max}$  are the nominal torque, stall torque, and maximum speed of the motor in joint  $i$ . Moreover,  $T_{g,i}$ ,  $T_{g,i}^{\max}$ , and  $N_{g,i}^{\max}$  are the rated output torque, maximum output torque, and maximum input speed of the gearbox in joint  $i$ . Among these constraints, Eqs. (26c)–(26e) apply to the motor selection, while Eqs. (26f)–(26h) are for the gearbox selection. The kinematic performance is constrained through Eq. (26b). So far, we have formulated the design problem as a discrete optimization problem, which can be solved by commercial available codes. We select a non-gradient method called Complex for this purpose. The implementation is outlined in the next section.

## 4. Procedure of optimization

After the problem of optimization is formulated, a discrete optimization algorithm, the Complex method, is used to solve the problem.

### 4.1. Optimization by the Complex method

The Complex method is a non-gradient based optimization method, first presented by Box [31]. With this method, a number of points (sets of design variables) will be evaluated against the objective function. The set of design variables minimizing the objective function is denoted as the best point  $\mathbf{x}_b$ , while the one maximizing the objective function is denoted as the worst point  $\mathbf{x}_w$ . Their corresponding values of the objective function are noted as the best and worst values. The candidate point is found by

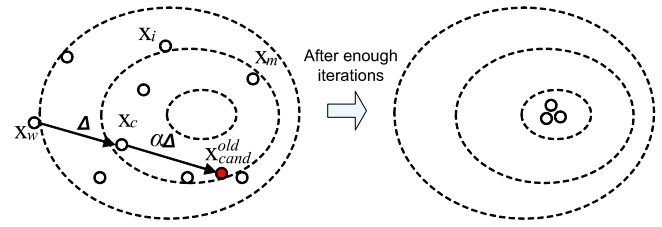


Fig. 4. Illustration of the complex method.

the reflection of the worst point through the centroid  $\mathbf{x}_c$  with a reflection coefficient  $\alpha$  (as shown in Fig. 4), yielding the following expression for the candidate design point.

$$\mathbf{x}_c = \frac{1}{m-1} \sum_{i=1}^m \mathbf{x}_i, \quad \mathbf{x}_i \neq \mathbf{x}_j \quad (27a)$$

$$\mathbf{x}_{cand}^{old} = \mathbf{x}_c + \alpha(\mathbf{x}_c - \mathbf{x}_w). \quad (27b)$$

To avoid converging at a local minimum, the candidate point can be modified as

$$\mathbf{x}_{cand} = \frac{1}{2}(\mathbf{x}_{cand}^{old} + \varepsilon \mathbf{x}_c + (1 - \varepsilon) \mathbf{x}_b) + (\mathbf{x}_c - \mathbf{x}_b)(1 - \varepsilon)(2K - 1) \quad (28)$$

where  $K$  is a random number varying in the interval  $[0, 1]$ , with

$$\varepsilon = \left( \frac{n_r}{n_r + k_r - 1} \right)^{\frac{n_r + k_r - 1}{n_r}}$$

Here  $k_r$  is the number of repeating times the point has repeated itself, and  $n_r$  is a parameter which is recommended as 4 in the program. The algorithm converges when the difference between the best and worst objective function values is less than a user defined tolerance.

### 4.2. Design variable programming

The design points in the Complex method are usually not integers. On the other hand, the design variables  $\mathbf{u}_m$  and  $\mathbf{u}_g$  have to be integral, since they are the index numbers from the categories of motors and gearboxes. Hereby, a round function is introduced to transfer the design variables into integral numbers. The round function is given as

$$x_{DV} = \text{round}(x) = \begin{cases} x_{int}; & \text{if } x_{int} \leq x < x_{int} + 0.5 \\ x_{int} + 1; & \text{if } x_{int} + 0.5 \leq x < x_{int} + 1 \end{cases} \quad (29)$$

where  $x$  is a design variable manipulated by the Complex method,  $x_{int}$  is the integral part of the number  $x$ , and  $x_{DV}$  is the rounded design variable.  $x_{DV}$  is used to update link lengths and the mass of motors and gearboxes in inverse kinematic and dynamic analysis.

### 4.3. The optimization routine

The implementation of the optimization takes two steps: implementation of the optimization routine and generation of a parametric simulation model. The optimization program is implemented in Matlab. The flow diagram of the optimization routine is shown in Fig. 5.

## 5. The arm design optimization

### 5.1. Initial arm trajectory

Design optimizations were conducted for the robot arm, using the integrated dimensional and drive-train optimization method. The initial arm trajectory in the base coordinate system is defined

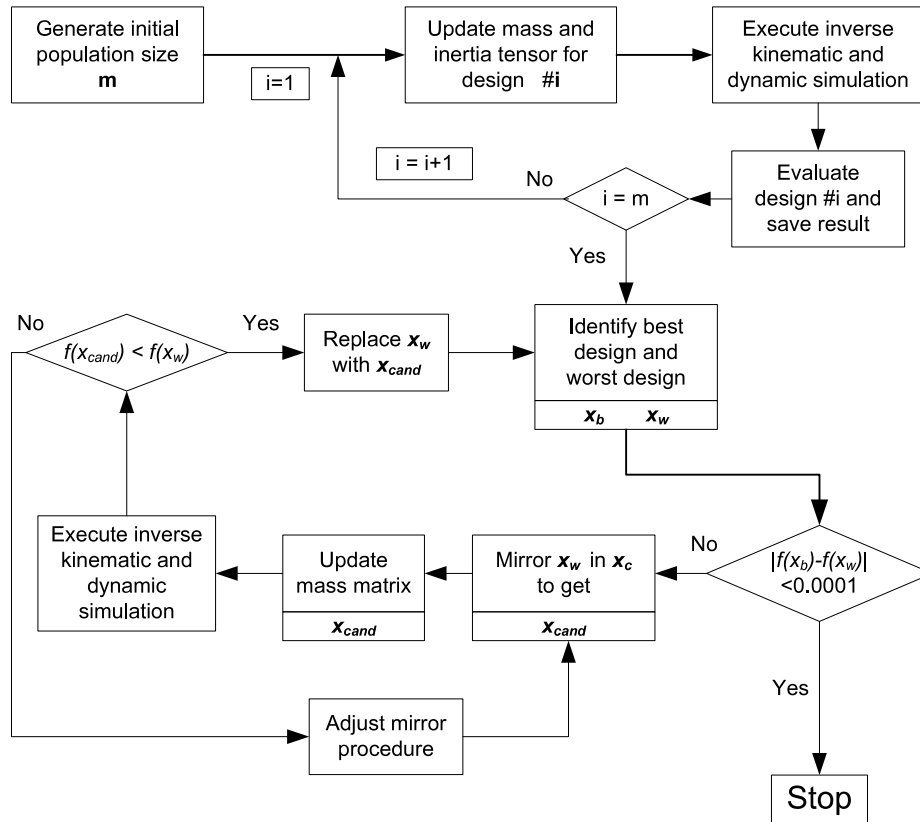


Fig. 5. Diagram of the optimization routine.

as  $X_{ef}(t) = 50 + 400(1 - \cos(t))$ ,  $Y_{ef}(t) = -1000 + 800(1 - \cos(t/2))$ , and  $Z_{ef}(t) = 280 + 250(\cos(t/2) - 1)$ , all with unit of mm. The Euler angles for the end-effector are given as  $[0, \cos(t/20), 0]$ , which implies the end-effector remains horizontal during the motion. The payload is defined as a point of mass of 5 kg.

### 5.2. Parameterized dimension

The variable geometric dimensions include the lengths of the upper arm  $l_1$  and lower arm  $l_2$  (in Fig. 2), while  $h_1$  and  $d_1$  are fixed. To keep the reachable space of the robotic arm constant, the total reaching distance  $L = l_1 + l_2$  is fixed.

One non-dimensional parameter  $r$  is introduced as  $r = l_1/L$ . Considering the structural issues, a minimum length is required for both lower and upper arms, which means

$$r \in [r_{\min}, r_{\max}]. \quad (30)$$

The link length ratio  $r$  is manipulated in the interval  $[r_{\min}, r_{\max}]$ , so there is infinite number of ratios theoretically. In practice, a vector  $\mathbf{r}$  is defined by discretizing  $r$  in the interval  $[r_{\min}, r_{\max}]$  with a step of  $Z = 0.05$ .

$$\mathbf{r} = \{r_{\min} + u_d \cdot Z\}_{u_d=1}^{u_d=c} \quad (31)$$

where  $u_d$  is an index number for this length ratio, and  $c = (r_{\max} - r_{\min})/Z + 1$ . In the case of optimization with multiple dimensions,  $u_d$  becomes an array of indices,  $\mathbf{u}_d$ , for dimensional variables.

### 5.3. Candidate components

The candidate components, including motors and gearboxes, can be defined by the designer on the basis of available products. In this work, the components are to be selected from Maxon motors

Table 2  
Candidate motor data from Maxon motor [27].

Index no.	Motor model	$T_m$ (Nm)	$T_m^{\max}$ (Nm)	$N_m^{\max}$ (rpm)	$J_m$ (g cm <sup>2</sup> )	$m_m$ (kg)
1	RE 25	0.0284	0.28	14,000	10.5	0.13
2	RE 26	0.0321	0.227	14,000	12.1	0.15
3	EC-i 40	0.0667	1.81	15,000	24.2	0.21
4	RE 30	0.0882	1.02	12,000	34.5	0.238
5	EC 32	0.0426	0.353	25,000	20	0.27
6	RE 35	0.0965	0.967	12,000	67.4	0.34
7	RE 36	0.0795	0.785	12,000	67.2	0.35
8	EC 40	0.127	0.94	18,000	85	0.39
9	RE 40	0.184	2.5	12,000	138	0.48

Table 3  
Candidate gearbox data from Harmonic Drive [32].

Index no.	CPU unit size	Ratio	$T_g$ (Nm)	$T_g^{\max}$ (Nm)	$N_g^{\max}$ (rpm)	$J_g$ (kg m <sup>2</sup> )	$m_g$ (kg)
1	14	100	11	54	8500	$0.033 \times 10^{-4}$	0.54
2	17	100	39	110	7300	$0.079 \times 10^{-4}$	0.79
3	20	100	49	147	6500	$0.193 \times 10^{-4}$	1.3
4	25	100	108	284	5600	$0.413 \times 10^{-4}$	1.95

and Harmonic Drives. To this end, nine candidate motors are selected. They are listed in the database ascendingly with respect to the mass of motor, as shown in Table 2. Moreover, four gearboxes from Harmonic Drive CPU units are selected and included in the database, as listed in Table 3. For the Harmonic Drive gearboxes, the efficiency is a function of operation speed. In this paper, the gear efficiency is set to 0.85 for all gearboxes, which is an average value from product catalog.

The gear ratio of each joint is set to  $\rho = \{200, 200, 200, 51, 100\}$ , orderly from Joint 1 to 5. Note there are two stage gearboxes in Joints 1, 2 and 3, a planetary gearhead and a Harmonic Drive unit. For simplicity, only the mass of the Harmonic Drive gearbox

**Table 4**  
Optimal link ratio and drive-train combinations for minimization of arm mass.

Joint	Initial		Optimized		Fixed $r = 0.5$	
	Motor	Gearbox	Motor	Gearbox	Motor	Gearbox
1	RE 40	CPU 17	EC 32	CPU 14	RE 35	CPU 14
2	RE 35	CPU 17	RE 25	CPU 14	RE 25	CPU 14
3	RE 35	CPU 17	RE 30	CPU 14	RE 35	CPU 14
4	RE 35	Gearhead	RE 25	Gearhead	RE 25	Gearhead
5	RE 35	CPU 17	RE 25	CPU 14	RE 25	CPU 14
Link ratio	$r = 0.5$		$r = 0.6$		$r = 0.5$	
Arm mass (kg)	16.7		9.92		9.98	

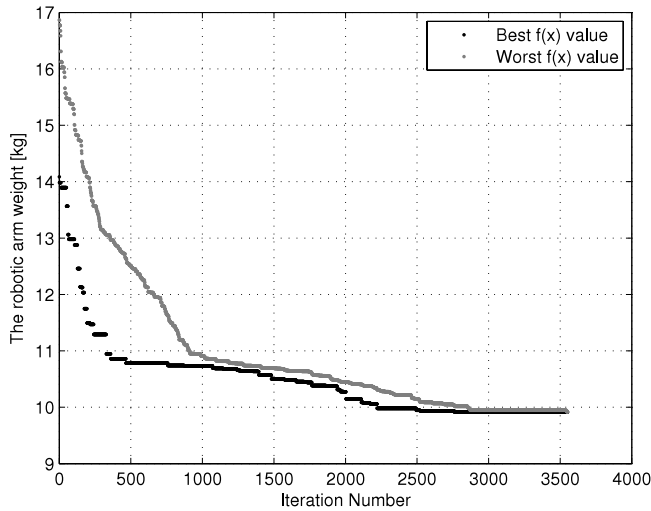


**Fig. 6.** Convergence of the mass of the robotic arm.

is parameterized, while the mass of the planetary gearhead is set to constant. The Harmonic Drive CPU unit is used in all joints except Joint 4, due to the joint structure consideration. A planetary gearhead is used in Joint 4, so  $u_{g,4} = 0$ .

#### 5.4. Optimization results

Once the candidate components have been selected, their corresponding limits of the inequalities (26c)–(26h) are determined. The limit of kinematic performance  $GCI$  is set to  $C_{\min} = 0.02$ , a limit that can be satisfied by a robotic arm with link ratios between  $r = 0.2 \sim 0.8$ . Optimized designs of motors and gearboxes for the robotic arm are listed in Table 4. The initial combination of motors and gearboxes are selected based on previous dynamics simulation of the robotic arm. The optimized mass of the robotic arm is 9.92 kg, with a reduction of 41% corresponding to the initial combinations. Another optimization case with fixed link length  $r = 0.5$  is also shown in Table 4 for comparison. In this design case, the mass change is not significant relative to the previous optimized case, but still noticeable. The change is due to the size of the motor at Joints 1 and 3. Referring to Table 2, the corresponding nominal torques are 0.0426 Nm (EC 32) and 0.0965 Nm (RE 35) for Joint 1.

The convergence of the objective function is depicted in Fig. 6, both best (black dot) and worst (gray dot) values from the Complex algorithm are shown. The solution to the optimal result is achieved at 3500 iterations with 130 population sizes. In this work, the tolerance of convergence is 0.0001.

The convergences of the link length ratio and  $GCI$  are shown in Figs. 7 and 8. The link length ratio is converged to  $r = 0.6$ . Fig. 9(a) illustrates the convergence of motor design variables. Only the convergence plots for Joints 1 and 5 are displayed for clarity. The convergence of gearbox design variables is depicted in Fig. 9(b). Comparing the convergence rates for the motor and gearbox design variables, the gearbox design variables converge faster toward the optimal results than the motor design variables. This phenomena

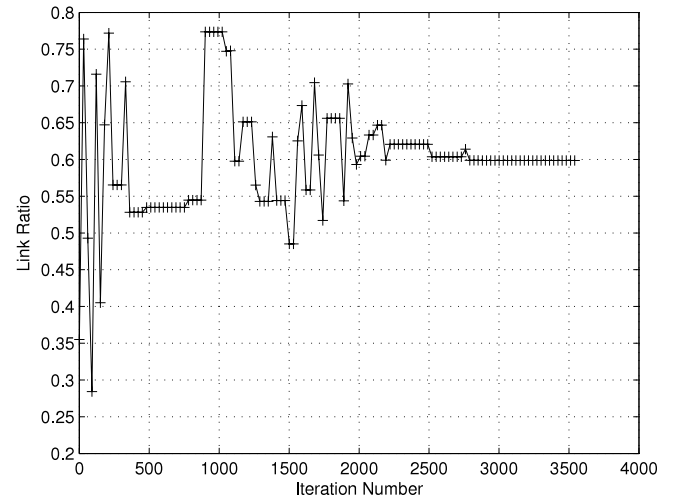


**Fig. 7.** Convergence of the link length ratio.

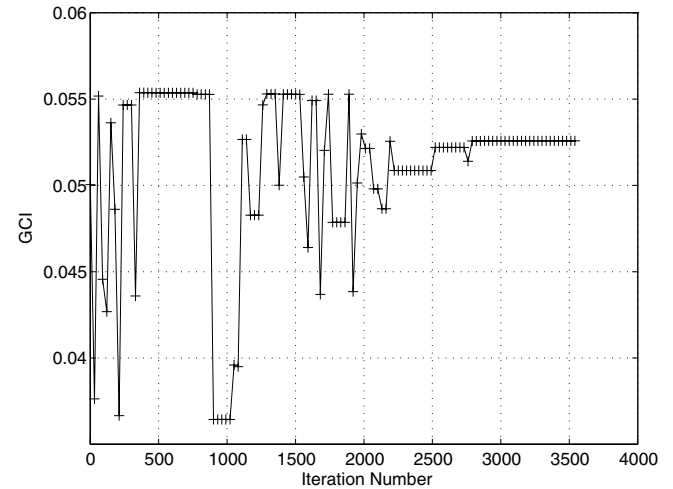


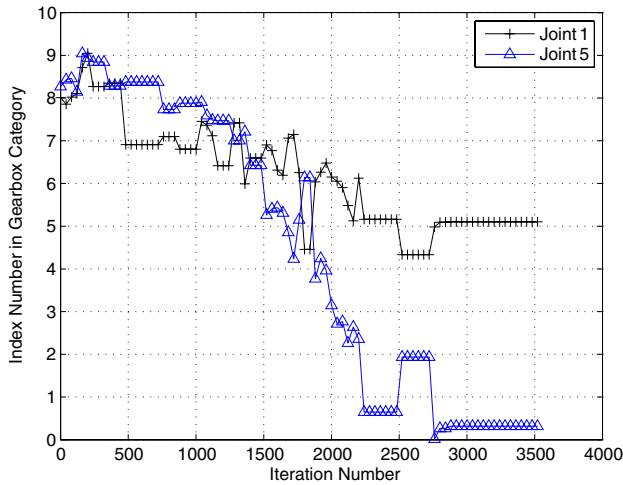
**Fig. 8.** Convergence of the  $GCI$  of the arm.

is caused by that the mass difference among Harmonic Drive units is larger than among motors.

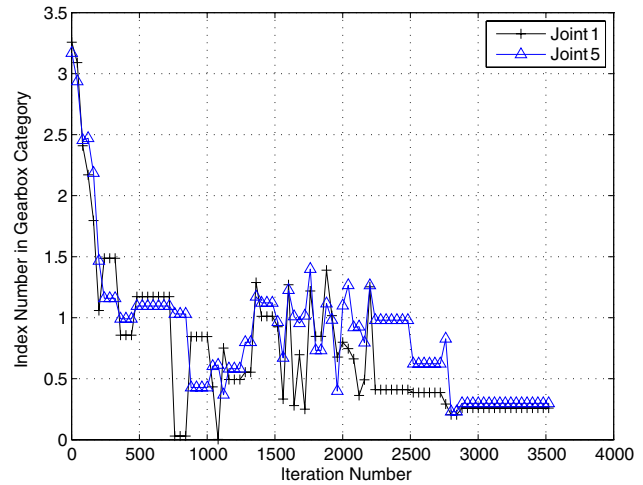
The variations of motor torques of Joints 1 and 2 for the initial and the optimal design are shown together in Fig. 10. The torques of the optimal design are depicted in black color, and that of the initial design are in gray. The RMS value of each torque is depicted with dashed line. It is seen that the optimal design has a reduction of 41.29% RMS torque for Joint 1, and a reduction of 26.87% RMS torque for Joint 2.

#### 5.5. Design optimization with an alternative trajectory

Another trajectory is used for the integrated optimization. This trajectory is given for a pick-and-place operation (PPO) defined

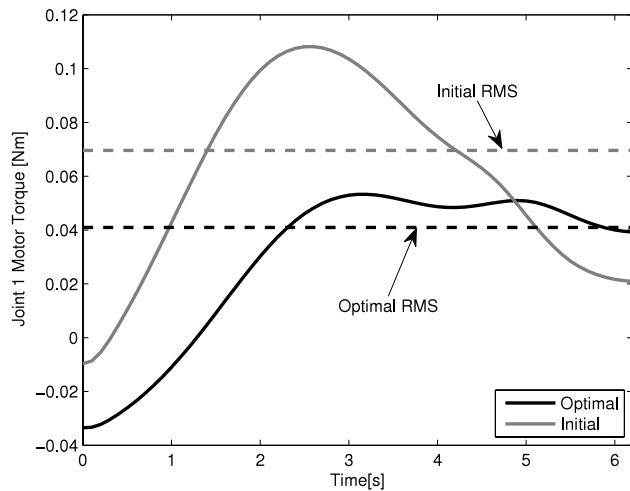


(a) Motors.

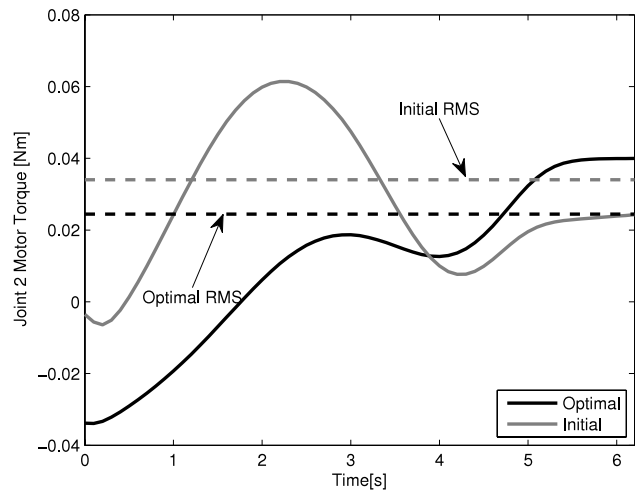


(b) Gearboxes.

Fig. 9. Convergence plots for the design variables of motors and gearboxes.



(a) Joint 1.



(b) Joint 2.

Fig. 10. Motor torques for initial and optimal drive-train combinations.

Table 5  
Optimization results for an alternative trajectory.

Joint	Motor	Gearbox
1	EC 32	CPU 14
2	EC-i 40	CPU 14
3	RE 25	CPU 14
4	RE 25	Gearhead
5	RE 25	CPU 14
Link ratio	$r = 0.6$	
Arm mass (kg)	9.85	

by  $X_{ef}(t) = 600$ ,  $Y_{ef}(t) = -150 \cos(t) - 150$ , and  $Z_{ef}(t) = 300 \cos(t/2) - 100$ , all with unit of mm, as depicted in Fig. 11. The duration is 6.2 s. The orientation for the end-effector is described by Euler angles  $[0, \cos(t/20), 0]$ , following the Z–X–Z convention.

Convergence of the mass of the robotic arm is depicted in Fig. 12. The solution to the optimal result is achieved at 3800 iterations with 130 population sizes. The optimization result for the alternative trajectory is listed in Table 5. The optimization with the alternative trajectory yields a design of mass slightly less than the case with the initial trajectory.

### 5.6. Optimization with a different GCI limit

Another optimization is conducted with  $C_{min} = 0.05$ . The trajectory utilizes the same one in Section 5.4. The convergence of the objective function is depicted in Fig. 13. The optimized mass is 9.88 kg. The solution to the optimal result is achieved at 3500 iterations, which implies the same converging rate as the case with  $C_{min} = 0.02$ .

The link length ratio is converged to  $r = 0.6$ . The variance of GCI during the optimization is shown in Fig. 14. The convergence result with  $C_{min} = 0.05$  is identical to the one with  $C_{min} = 0.02$ , as shown in Figs. 6 and 8.

### 5.7. Discussions

By comparing the optimization results for two trajectories (Tables 4 and 5), it can be seen that the minimum mass changes slightly, while the integrated optimization method yields different combinations of motors and gearboxes. On the other hand, the link length ratio of the arm structure remains unchanged. This suggests that the design optimization with the selected trajectories is practical. The results generated from a worst case identified by the first trajectory is able to fulfill dynamic requirements in normal manipulations.

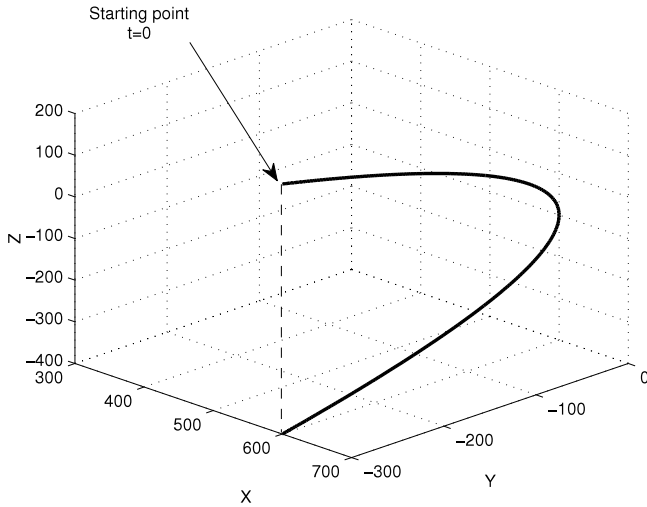


Fig. 11. Illustration of the alternative trajectory.

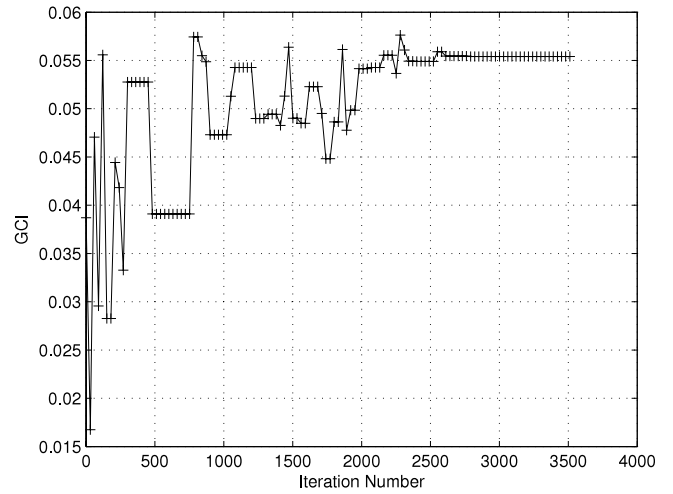


Fig. 14. Convergence of the GCI of the arm for  $C_{min} = 0.05$ .

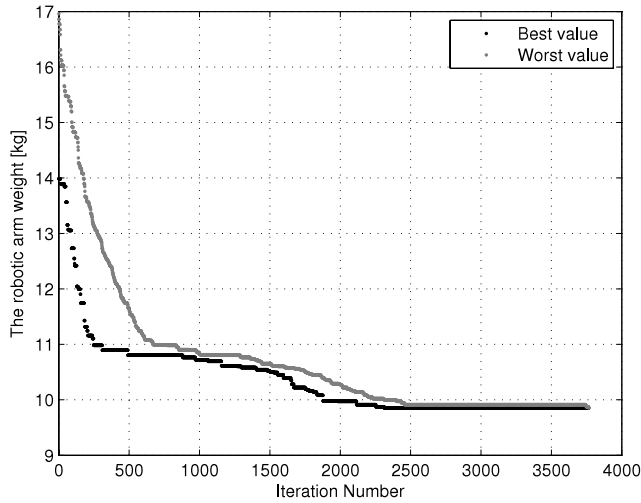


Fig. 12. Convergence of the mass of the robotic arm for the alternative trajectory.

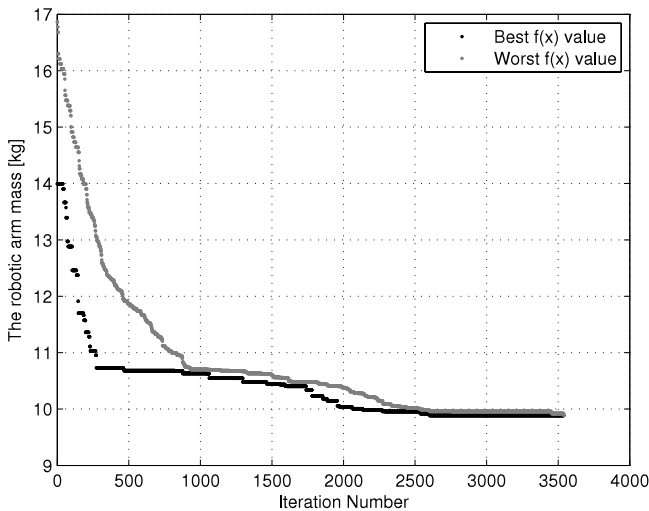


Fig. 13. Convergence of the mass of the robotic arm for  $C_{min} = 0.05$ .

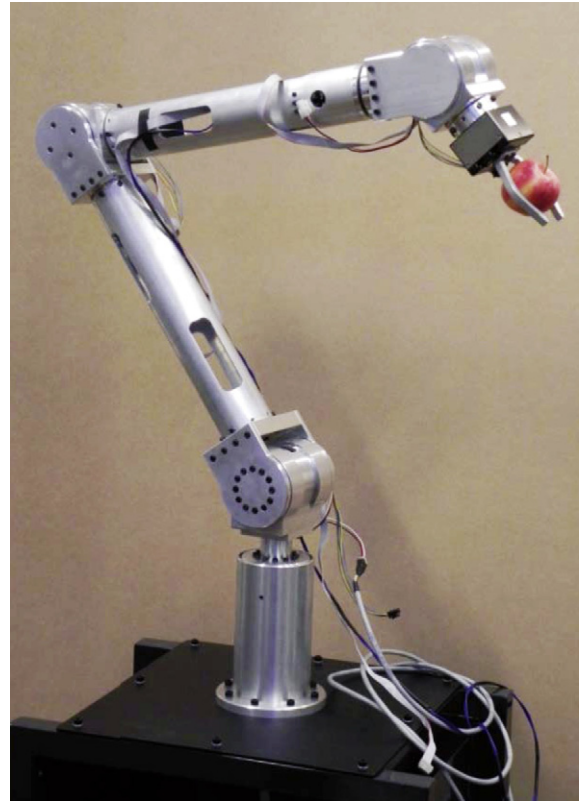


Fig. 15. Prototype of the 5-dof robotic arm.

The optimal link length ratio for both trajectories and different GCI limits is  $r = 0.6$ . Comparing this ratio to some robotic manipulators [25] such as KUKA-KR-R650 ( $r = 0.55$ ), Denso-VM-6083D series ( $r = 0.54$ ), Mitsubishi-RV-2AJ series ( $r = 0.61$ )

and Staubli-TX40 series ( $r = 0.58$ ), the optimal ratio agrees generally with these industrial robots. The difference between these ratios can be considered as the influence on arm shape and mass distributions. The prototype of the 5-dof robotic arm in this work is shown in Fig. 15. The components of drive-train in the prototype are selected and scaled based on the optimization results.

While the integrated dimensional and drive-train design optimization was done on a platform developed with Matlab, the method can be applied to commercial available CAD/CAE systems. To this end, dynamics simulation will be implemented in a CAE system, e.g. MSC.ADAMS™. On the other hand, Matlab program will serve as an interface between the user and CAD/CAE systems and run the Complex routine. In this way, the method can easily

be extended to include other constraints, for example, strength constraints evaluated by FEA software like ANSYS™.

The proposed approach is aimed for the off-the-shelf design of a robotic arm, for which the drive-train components are standard commercial products. This implies that the performance (weight) improvement with the developed method may be limited for light-weight robot designs with customer designed actuators, as the case of DLR light-weight arm, for which the challenges lie in the novel motor design, topology optimization and new materials, rather the problems addressed in this work.

## 6. Conclusions

An integrated dimensional and drive-train optimization method was proposed for the design of robotic manipulators. Selections of geometric dimensions, motors and gearboxes were formulated as a discrete optimization problem, which was solved by a non-gradient optimization method. Global conditioning index was taken as constraint on kinematic performance of the robot. The robot dynamics was constrained by considering characteristics of motors and gearboxes. The proposed method is able to reach a design with lower mass and optimal geometric dimensions. A 5-dof light-weight anthropomorphic robotic arm was designed by implementing the presented method. Case studies were conducted to demonstrate the application of the method in the design of robotic manipulators. The optimal design is able to fulfill dynamic requirements in normal operations. In the future works, constraints will be extended to include considerations such as strength/stiffness and energy consumptions.

## Acknowledgments

The project is sponsored by Aalborg University and Det Obelske Familiefond (DOF). The authors appreciate anonymous reviewers for their helpful comments and suggestions to improve the quality of the article.

## References

- [1] O. Ivlev, C. Martens, A. Graeser, Rehabilitation robots FRIEND-I and FRIEND-II with the dexterous lightweight manipulator, *Technology and Disability* 17 (2005) 111–123.
- [2] Z. Bien, M.J. Chung, P.H. Chang, D.S. Kwon, Integration of a rehabilitation robotic system (KARES II) with human-friendly man-machine interaction units, *Autonomous Robots* 16 (2004) 165–191.
- [3] R.M. Mahoney, The Raptor wheelchair robot system, in: M. Mokhtari (Ed.), *Integration of Assistive Technology in the Information Age*, IOS press, 2001, pp. 135–141.
- [4] A. Albu-Schäffer, S. Haddadin, C. Ott, A. Stemmer, T. Wimböck, G. Hirzinger, The DLR lightweight robot: design and control concepts for robots in human environments, *Industrial Robot* 34 (5) (2007) 376–385.
- [5] A. Jardon, A. Gimenez, R. Correal, R. Cabas, S. Martinez, C. Balaguer, A portable light-weight climbing robot for personal assistance applications, *Industrial Robot* 33 (4) (2006) 303–307.
- [6] A. Ananiev, D. Ignatova, B. Iliev, An approach to the design of a light-weight reconfigurable robot arm for a mobile robot, *Problems of Engineering Cybernetics and Robotics* 53 (2002) 93–100.
- [7] B. Rooks, The harmonious robot, *Industrial Robot* 33 (2) (2006) 125–130.
- [8] P. Chedmail, M. Gautier, Optimum choice of robot actuators, *Journal of Engineering for Industry* 112 (1990) 361–367.
- [9] M. Petterson, J. Ölvander, Drive train optimization for industrial robots, *IEEE Transactions on Robotics* 25 (6) (2009) 1419–1423.
- [10] H. Elmqvist, H. Olsson, S.E. Mattsson, D. Brück, Optimization for design and parameter estimation, in: *Proceedings of the 4th International Modelica Conference*, 2005, pp. 255–266.
- [11] L. Zhou, M.R. Hansen, S. Bai, Drive train design optimization of a 5-dof light-weight robotic arm, in: *Proceedings of the 1st Joint International Conference on Multibody System Dynamics*, Lappeenranta, Finland, 2010.
- [12] P.S. Shiakolas, D. Koladiya, J. Kebrle, Optimum robot design based on task specifications using evolutionary techniques and kinematic, dynamic, and structural constraints, *Inverse Problems in Science and Engineering* 10 (4) (2010) 359–375.
- [13] B.K. Rout, R.K. Mittal, Optimal design of manipulator parameter using evolutionary optimization techniques, *Robotica* 28 (2010) 381–395.
- [14] A. Bowling, O. Khatib, Dynamic loading criteria in actuator selection for desired dynamic performance, *Advanced Robotics* 17 (7) (2003) 641–656.
- [15] Z. Shiller, S. Sundar, Design of robotic manipulators for optimal dynamic performance, in: *Proceedings of the 1991 IEEE International Conference on Robotics and Automation*, 1991, pp. 344–349.
- [16] O. Khatib, J. Burdick, Optimization of dynamics in manipulator design: the operational space for formulation, *International Journal of Robotics and Automation* 2 (2) (1987) 90–98.
- [17] D.-Z. Chen, Drive train configuration arrangement for gear coupled manipulators, *Journal of Robotic Systems* 14 (8) (1997) 601–612.
- [18] J. Denavit, R.S. Hartenberg, A kinematic notation for lower pair mechanisms based on matrices, *ASME Journal of Applied Mechanics* 77 (1955) 215–221.
- [19] L.W. Tsai, *Robot Analysis: The Mechanics of Serial and Parallel Manipulators*, John Wiley & Sons, 1999.
- [20] T. Yoshikawa, Manipulability of robotic mechanisms, *The International Journal of Robotics Research* 4 (2) (1985) 3–9.
- [21] C. Gosselin, J. Angeles, A global performance index for the kinematic optimization of robotic manipulators, *ASME Journal of Mechanical Design* 113 (1991) 220–226.
- [22] J.K. Salisbury, J.J. Craig, Articulated hands: force control and kinematic issues, *The International Journal of Robotics Research* 1 (1) (1982) 4–17.
- [23] C. Gosselin, J. Angeles, The optimum kinematic design of a planar three-degree-of-freedom parallel manipulator, *ASME Journal of Mechanisms, Transmissions, and Automation in Design* 110 (1) (1988) 35–41.
- [24] C. Gosselin, The optimum design of robotic manipulators using dexterity indices, *Robotics and Autonomous Systems* 9 (4) (1992) 213–226.
- [25] S. Kucuk, Z. Bingul, Comparative study of performance indices for fundamental robot manipulators, *Robotics and Autonomous Systems* 54 (2006) 567–573.
- [26] S. Bai, Optimum design of spherical parallel manipulators for a prescribed workspace, *Mechanism and Machine Theory* 45 (2010) 200–211.
- [27] Maxon motor products catalogue 10/11, Available from: [www.maxonmotor.ch/e-paper/blaetterkatalog/pdf/complete.pdf](http://www.maxonmotor.ch/e-paper/blaetterkatalog/pdf/complete.pdf).
- [28] Engineering data for harmonic drive gears, Available from: [www.harmonicdrive.de/cms/upload/pdf/en/cpu\\_h7.pdf](http://www.harmonicdrive.de/cms/upload/pdf/en/cpu_h7.pdf).
- [29] R.L. Norton, *Machine Design: An Integrated Approach*, 4th edition, Prentice Hall, 2010.
- [30] G.G. Antony, Rating and sizing of precision low backlash planetary gearboxes for automation motion control and robotics applications, Available from: [www.neugartusa.com/Service/faq/Gear\\_Rating.pdf](http://www.neugartusa.com/Service/faq/Gear_Rating.pdf).
- [31] M.J. Box, A new method of constrained optimization and a comparison with other methods, *Computer Journal* 8 (1965) 42–52.
- [32] Harmonic drive technical data, Available from: [www.harmonicdrive.de/cms/upload/German/B\\_Produnkte/B\\_Units/kompl\\_Produktkapitel\\_CPU\\_D-E.pdf](http://www.harmonicdrive.de/cms/upload/German/B_Produnkte/B_Units/kompl_Produktkapitel_CPU_D-E.pdf).



**Lelai Zhou** received his B.Eng. in Mechanical Engineering and Automatization in 2006 from the University of Science and Technology, Beijing, China, and his M.Eng. in Mechanical Design and Theory in 2009 from Beihang University, China. He is currently a Ph.D. Student in the Department of Mechanical and Manufacturing Engineering at Aalborg University. His main research is robotic arm design optimization and control.



**Shaoping Bai** received the Ph.D. Degree in Mechanical and Production Engineering from the Nanyang Technological University, Singapore in 2001, the M.Eng. Degree from Tsinghua University and B.S. Degree from Harbin Institute of Technology in 1993 and 1988, respectively. He is currently an Associate Professor at the Department of Mechanical and Manufacturing Engineering, Aalborg University (AAU), Denmark. His research interests include dynamics and design, medical and assistive robots, parallel manipulators, and walking robots. He is a member of ASME and IEEE Robotics and Automation.



**Michael Rygaard Hansen** is currently holding a position as Professor in Fluid Power in the Mechatronics group within the Department of Engineering at the University of Agder since 2009. His main research interests lie within:

- design optimization
- modeling and time domain simulation of hydraulically and electrically actuated machinery
- dynamics of hydraulically and electrically actuated machinery.

MRH took his M.Sc. (1989) and Ph.D. (1992) at the Institute of Mechanical Engineering at Aalborg University where he also held a position as Assistant Professor 1992–1995 and Associate Professor in 1995–1997 and 1999–2008. MRH has several years of experience from industry including spells at Danfoss Mobile Hydraulics (part of Danfoss A/S), 1997–1999 and Aker Marine Hydraulics (part of Aker Solutions AS), since 2009.